Energy Conversion and Management 326 (2025) 119506

Contents lists available at ScienceDirect

Energy Conversion and Management

journal homepage: www.elsevier.com/locate/enconman

Research Paper

Thermoeconomic analysis of an integrated membrane reactor and carbon dioxide capture system producing decarbonized hydrogen

Yagmur Nalbant Atak [a,*], Alper Can Ince [b,c], C.Ozgur Colpan [d,e], Adolfo Iulianelli [f,*], Mustafa Fazil Serincan [c], Ugur Pasaogullari [b,c]

[a] Atilim University, Faculty of Engineering, Department of Mechanical Engineering, Incek, Ankara 06836, Turkey
[b] Center for Clean Energy Engineering, University of Connecticut, Storrs, CT 06269-5233, USA
[c] Department of Mechanical Engineering, University of Connecticut, Storrs 191 Auditorium Road, Storrs, CT 06269-4602, USA
[d] Dokuz Eylul University, Faculty of Engineering, Mechanical Engineering Department, Buca Izmir, Turkey
[e] Dokuz Eylul University, Energy Application and Research Center (EUAM), Buca, Izmir, Turkey
[f] Institute on Membrane Technology of the National Research Council of Italy (CNR-ITM), Via P. Bucci, Cubo 17C, Rende 87036, Italy

ARTICLE INFO

Keywords:
Membrane reactor
Hydrogen production
CO_2 capture
Exergy
Techno-economic analysis

ABSTRACT

In this study, a novel thermo-economic analysis on a membrane reactor adopted to generate hydrogen, coupled to a carbon-dioxide capture system, is proposed. Exergy destruction, fuel, and environmental as well as purchased equipment costs have been accounted to estimate the cost of hydrogen production in the aforementioned integrated plant. It has been found that the integration of the CO_2 capture system with the membrane reactor is responsible for the reduction of the hydrogen production cost by 12 % due to the decrease in environmental penalty cost. In addition, the effects of operating parameters (steam-to-carbo ratio and biogas temperature) on the hydrogen production cost are investigated. Hence, this work demonstrates that the latter can be decreased by approximately 2 $\$/kg_{H_2}$ when steam to carbon ratio increases from 1.5 to 4. The analyses reveal that steam-to-carbo ratio increases exergy destruction cost, affecting consequently also the hydrogen production cost. However, from a thermodynamic point of view, it enhances the hydrogen production in the membrane reactor, mutually lowering the hydrogen production cost. It has been also estimated that a decrease in the biogas inlet temperature from 450 to 400°C can reduce the hydrogen production cost by 7 %. This study demonstrates that the fuel cost is a major economic parameter affecting commercialization of hydrogen production, while exergy destruction and environmental costs are also significant factors in determining the hydrogen production cost.

1. Introduction

The importance of hydrogen production as a new and carbon-free energy vector is growing up quickly, with the intent of promoting a sustainable energy future contrasting the disadvantages due to the utilization of fossil fuels, which impact greatly on the environment in terms of air pollution, and global warming as well. Fossil fuels present also limited availability, they are subjected to depletion, and reliance on imports [1,2]. Hydrogen can be produced using various methods (thermochemical, electrolytic, biological, and photonic), depending on the primary energy source (renewable electricity, fossil fuels, natural gas, nuclear electricity, etc.), resulting in different CO_2 footprint (1–20 kg_{CO_2}/kg_{H_2}) and manufacturing cost (between 0.5–10 $\$/kg_{H_2}$) [3]. When hydrogen is produced from renewable energy sources with zero emissions, the product is defined roughly as green hydrogen; whereas when it is produced from fossil fuels and integrated with the CO_2 capture and storage, it is defined as blue hydrogen. Blue and green hydrogen constitute promising solution to overcome the disadvantages of fossil fuels exploitation, supporting the decarbonization, enabling a clean energy storage, helping in grid balancing, and providing economic growth in the renewable energy sector [1,2].

Membrane reactor (MR) technology, which provides simultaneous hydrogen production and separation within a single device, plays a key role in integrated hydrogen technologies (e.g., fuel cells and power-to-gas applications). When the MRs are compared to conventional reactors, they show several advantages such as enhanced reaction kinetics, simplified process flows, improved hydrogen purity, compactness, feedstock flexibility, and need of relatively milder operating conditions [4]. In MRs, hydrogen is removed continuously from the reaction side to

* Corresponding authors.
E-mail addresses: yagmur.atak@atilim.edu.tr (Y.N. Atak), a.iulianelli@itm.cnr.it (A. Iulianelli).

https://doi.org/10.1016/j.enconman.2025.119506
Received 16 October 2024; Received in revised form 9 January 2025; Accepted 9 January 2025
Available online 17 January 2025

Nomenclature

A_c	Cross sectional area, m^2
B_{H_2}	Hydrogen permeability, mol/(s·m^2·Pa^n)
c	Cost per unit exergy, $/kWh
$\overline{c}_p$	Specific heat constant, J/mol·K
CR_{cat}	Cost of the catalyst per unit volume, $/$m^3$
CRF	Capital recovery factor
DEN	The coefficient of the adsorption of reacting species onto the active catalyst sites
DF	Depreciation factor
EC	Electricity cost, $/kWh
E_i	Activation energy of reaction, i
$\dot{E}x$	Exergy rate, W
$\dot{E}x_D$	Exergy destruction rate, W
F_m	Material factor
F_n	Pressure factor
F_p	Proportionality constant that accounts for changes in the reactor pressure and materials
g	Gravitational acceleration, m/s^2
$\overline{h}_i$	Specific molar enthalpy of i, J/mol
$\Delta\overline{H}_i$	Molar enthalpy change of reaction i, J/mol
i_r	Interest rate, %
J_{H_2}	Hydrogen permeation flux, kmol/(m^2·h)
$k_{0,i}$	Pre-exponential factor for i^{th} reaction, kmol·$bar^{0.5}$/(kg_{cat}·h)
K_j	Adsorption constant for species, j
$K_{j,0}$	Pre-exponential factor for adsorption constant
Keq_i	Equilibrium constant of reaction, i
LHV	Lower heating value, J/kg
MW	Molecular weight, kg/kmol
n	Predicted life of the component, year
$\dot{n}$	Molar flow rate, mol/ s
N	Operation hours per year, h
$\dot{Q}$	Heat transfer rate, W
p_j	Partial pressure of species j, bar
r	Radius, m
$\overline{R}$	Gas constant, kJ/kmol·K
R_i	Reaction rate of reaction i, kmol/(kg_{cat}-h)
t_{op}	Operational time, hour/year
T	Temperature, K
T_0	Reference temperature, K
U	Overall heat transfer coefficient, W/(m^2·K)
V	Velocity, m/s
Vol	Volume, m^3
$\dot{W}$	Power, W
z	Length of the reactor, m
Z_k	Purchase equipment cost for each k component, $
$\dot{Z}_k$	Initial cost rate, $/h

List of Greek letters

δ	Thickness, m
ν	Stoichiometric coefficient, –
ρ_b	Catalyst density, kg/m^3
φ	Maintenance rate

List of Subscripts and Superscripts

cat	Catalyst
comp	Compressor
cv	Control volume
CH_4	Methane
CO	Carbon monoxide
CO_2	Carbon dioxide
e	exit
f	fuel
fr	frame
H_2	Hydrogen
H_2O	Water
HEX	Heat exchanger
i	Reaction number
in	Input
j	Species
LHV	Lower heating value
mem	Membrane
MR	Membrane reactor
O&M	Operation and maintenance
O_2	Oxygen
0	Reference value
perm	Permeate
reac	Reaction
ret	Retentate
sep	Seperation
sys	System
SMR	Steam-methane reformer
S/C	Steam-to-carbon ratio
WGS	Water-Gas Shift

the permeation side by permeation through a hydrogen perm-selective membrane, enabling higher fuel conversions and improved hydrogen yields, leading to increased reactor efficiency [3,5–7]. Consequently, MR technologies contribute to advancing hydrogen production and promoting transition towards a cleaner and sustainable energy future [3,7]. From an economic point of view, MR systems represent an intensified solution not requiring further devices to generate high grade hydrogen. However, the conventional systems typically include four different steps such as steam-methane reformer (SMR) reactor, two water–gas shift (WGS) reactors, and a purification unit. Therefore, MRs can be simply integrated into several advanced and already existing systems (fuel cells, power-to-gas/liquid, etc.,), enhancing overall economic performance compared to conventional plants [8]. From an environmental point of view, MRs can be more suited to operate with CO_2 capture devices compared to conventional systems since MRs do not require additional chemical steps to separate hydrogen from CO_2. Thus, the energy conversion process can be targeted to reach low/zero CO_2 emissions and increase energy efficiency, and MR integrated plants providing simultaneous hydrogen production and CO_2 capture are accepted as one of the most promising and sustainable technological strategies [9,10].

In literature, there are a number of studies focusing on the integration of MRs used for hydrogen production with other technologies. In an experimental study dealing with the MR coupling with CO_2 capture systems, Wu et al. [11] studied a CO_2 perm-selective MR for producing hydrogen from methane by steam reforming process. This study shows that in situ CO_2 removal from the reactor positively affects the conversion rate of WGS reaction and increases the yield of hydrogen. In particular, hydrogen yield and CO_2 recovery at 900 °C and 1 atm were found 90 % and 84 %, respectively. Kian et al. [12] experimentally studied low-carbon hydrogen production with CO_2 capture using a Pd-based metallic MR and investigated its performance in terms of methane conversion, hydrogen purity, recovery, and CO and CO_2 selectivity at 400 °C and 1–4 bar. The results showed that, when the pressure increases from 1 bar to 4 bar, methane conversion increased from 23 % to 42 %. Furthermore, at 4 bar, the purity of the hydrogen

recovered in the permeate stream resulted to be > 99.999 %, meanwhile capturing up to 80 % of the CO_2 produced during the steam methane reforming. Kim et al. [13] experimentally studied hydrogen production from methane with a MR housing a Pd-based composite membrane to recover high grade hydrogen in the permeate and analysing whether the retentate gas is suitable to be used in CO_2 capture systems. This study showed that the hydrogen purity on the permeate stream was ~ 98 %, whereas CO_2 and CH_4 compositions in the retentate stream resulted to be ~ 68 % and 22 %, respectively. In addition, methane conversion and hydrogen recovery at 500 °C were 79.5 % and 98.7 %, respectively.

Some theoretical studies have dealt with mathematical models to simulate the integration of MRs with CO_2 capture systems. For example, Shirasaki et al. [14] conducted a case study about the integrated system used for producing high grade hydrogen by MR and, simultaneously, capturing CO_2 at the Tokyo Gas Company. This company developed a large-scale MR producing 40 Nm^3/h of high-grade hydrogen with 90 % of CO_2 concentration in the MR retentate stream, designing an integrated apparatus for CO_2 capture consisting of a gas–liquid separator, a gas compressor, a tank, and a chiller. In the hydrogen production process with only 3 % of energy loss, the emissions of CO_2 were decreased by 50 %. They developed a mathematical model for this system and the results showed that the system efficiencies to produce hydrogen with and without CO_2 capture were simulated to be 78.6 % and 81.4 %, respectively. Ma et al. [8] developed models using a Monte Carlo simulator for different case studies (conventional and MRs with and without a CO_2 capture system) to examine the economic performance of the integrated system. Analysing the case related to the increase of the carbon price, the sensitivity degree of economic performance in the case of hydrogen production by a conventional reactor adopting a CO_2 capture system results to be higher than that of a conventional reactor not adopting a CO_2 capture system. Lee et al. [16] conducted a comparative technoeconomic analysis for the sorption-enhanced MR (SEMR) providing simultaneous hydrogen production and CO_2 capture. In particular, both thermodynamic and economic studies were carried out with sensitivity and uncertainty analyses to estimate costs in detail. The results showed that hydrogen production costs by conventional reactor, MR, and SEMR resulted to be 4.53, 1.98, and 3.04 $\$/kg_{H_2}$, respectively. Furthermore, they found that the utilization of a SEMR for next-generation hydrogen production and CO_2 capture can be preferable due to a lower CO_2 emission rate than the others, although MR showed the lowest cost of hydrogen production. In our previous work, a thermodynamic analysis (energy and exergy) of an integrated system including an MR and a CO_2 capture system to produce decarbonized hydrogen was carried out [15]. The effects of operating parameters (temperature, pressure, and steam-to-carbon ratio) on the system performance (thermal efficiency, methane conversion, hydrogen yield, and CO_2 yield) and exergy destruction for each component were investigated, and the simulations showed that the best achievable methane conversion, hydrogen and CO_2 yields have been 51 %, 67 %, and 22 %, respectively. Thermal efficiency at 500 °C and 9 bar was found equal to 51 %.

However, to the best of our knowledge, no studies cover exergy and thermo-economic analyses of integrated plants consisting of a MR coupled to a CO_2 capture system, realising also a balance of plant components. Therefore, as an advancement of our previous publication [15], the novelty of this work deals with a comprehensive thermo-economic analysis on a MR adopted to generate high grade hydrogen by steam reforming of synthetic biogas, integrated with a CO_2 capture system. Moreover, an exergy analysis, as a consequence of the variation of key operating parameters, such as steam-to-carbo ratio and biogas inlet temperature, is proposed, further studying how the latter aspects may impact the costs of the integrated plant.

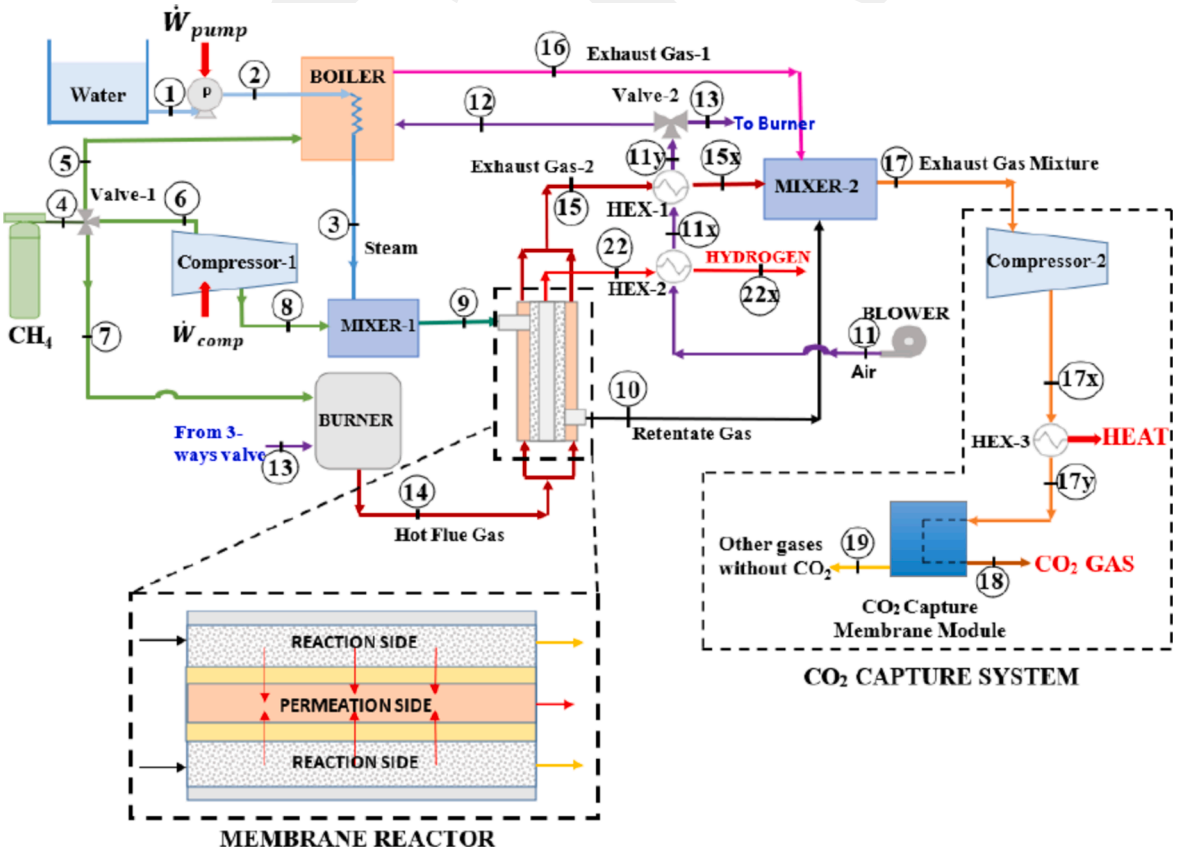

Fig. 1. Schematics of the integrated system producing decarbonized hydrogen and capturing CO_2 from the flue gases.

2. System description

Fig. 1 shows the schematic of the integrated plant producing decarbonized hydrogen and capturing CO_2 from the waste gases (hot flue gases from the burner and the exhaust gases from the boiler and MR). The plant consists of a MR, CO_2 capture system (compressor, heat exchanger, and membrane separation unit), and auxiliary plant components (compressor for methane, boiler, burner, water pump, air blower, and two mixers). In the layout of the integrated system two heat exchangers (HEX-1 and HEX-2) are used to heat the air leaving the blower (State 11); then the air splits into two streams in Valve-2: one stream goes to the burner (State 13) and the other one enters the boiler (State 12). Methane, as the main component of biogas, is fed to the boiler (State 5), compressor-1 (State 6), and burner (State 7) by a three-ways valve (State 4). Water is fed to the system from a pump (State 1), it is heated in the boiler and then the steam is fed to Mixer-1 (State 3) to be mixed with the methane coming from Compressor-1 (State 8). The feed gas consisting of methane and steam (State 9) is fed to the reaction side of the MR, where the steam-methane reforming, water gas shift, and direct steam methane reforming take place in the presence of a catalyst. The produced hydrogen in the reaction side permeates through the hydrogen perm-selective membrane and is collected in the permeation side.

The permeated hydrogen (State 22) comes out from the MR and enters the heat exchanger to heat up the air coming from the blower.

The required heat to drive the endothermic chemical reactions is provided from the hot flue gas coming from the burner (State 14) and fed to the jacket of the MR. The overall waste gases including the exhaust gas-1 from the boiler (State 16), the exhaust gas-2 from the burner (States 15x), and the retentate gas from MR (State 10) have different composition of gases (hydrogen, methane, CO, CO_2, N_2, and water). The waste gases are mixed in the Mixer-2 (State 17) and then fed to the CO_2 capture system to separate CO_2. At this stage, firstly, the gaseous mixture is fed to Compressor-2 to increase their pressure and then enters the heat exchanger (State 17x) to decrease their temperature. Finally, CO_2 is separated from the gaseous mixture by a polymeric membrane-based module operated at constant temperature and pressure. The captured CO_2 from the integrated system (State 18) could be potentially utilized in a power-to-X scheme, or in agriculture or as chemical feedstock [17]. In addition, the heat extracted from the heat exchanger used in the CO_2 capture system can be stored for later use in any application (e.g., district heating, cogeneration, space heating and cooling, water heating, or steam generation).

3. Mathematical modeling

In this section, the modeling equations of the main components of the system described in Section 2 are presented. A 1-D mathematical modeling of the MR was developed and validated in the previous study [15]. The other components and CO_2 capture system are investigated using a thermodynamic model. To find thermodynamic properties (e.g., enthalpy and entropy), the energy transfers (work and heat), and the exergy destructions of each component, mass, energy, and exergy balance equations are applied to the control volume of components in the integrated plant. In the MR, the reaction kinetics and Sievert's law are used to find the hydrogen production in the MR, hydrogen permeation through the membrane, and the reaction rates of steam methane reforming reactions [6,7]. In the burner and boiler, the molar ratio of hot flue gas and exhaust gas-1 produced in the burner and boiler, respectively, is calculated using the reaction kinetics equations. Moreover, the cost balance incorporated with the exergy balance is applied to each component to estimate the hydrogen production cost. All model equations are solved using MATLAB. The main assumptions used in the mathematical modeling of the integrated plant are reported below:

- The integrated system operates under steady-state conditions.
- All gases are treated as ideal gases.
- In the burner and boiler, complete burning occurs.
- Dry air composition used in the burner and boiler is taken as 21 % O_2 and 79 % N_2.
- The perm-selectivity of the dense self-supported tubular Pd-Ag membrane [18] housed in the MR is 100 % toward hydrogen.
- The membrane separation unit in the CO_2 capture system operates at a constant temperature and pressure.
- The walls of each component and the connection lines are thermally insulated.
- The flow rate of methane is taken as constant.
- Reactor inlet temperature is kept constant.

3.1. Component models

3.1.1. Membrane reactor

The details of the 1-D MR model and its validation are provided in our previous study [15]. In this subsection, the summary of the main model equations used in the MR is given. In the MR configuration analyzed in this work, the steam reforming reaction takes place in the MR shell side, whereas the produced hydrogen is collected in the membrane core. In the reaction side, the feed (methane and water) is fed to a Ni-based catalytic bed, and then the following reaction mechanism (Eqs. (1) − (3)) has been assumed to take place.

$$CH4 + H2O \rightarrow CO + 3H2 \quad \Delta\bar{h}_1 = 206,000 J/mol \tag{1}$$

$$CO + H2O \rightarrow CO2 + H2 \quad \Delta\bar{h}_2 = -41,000 J/mol \tag{2}$$

$$CH4 + 2H2O \rightarrow CO2 + 4H2 \quad \Delta\bar{h}_3 = 165,000 J/mol \tag{3}$$

Part of produced hydrogen permeates through the hydrogen perm-selective membrane from the reaction side to the permeate side [20]. The retentate gases, including methane, CO_2, CO, residual hydrogen, and steam, come out from the outlet stream of the reaction side. The mass and energy balance equations, and the hydrogen permeation equation as well for the MR reaction and permeation sides are, respectively, provided in Table 1.

The values of all constants used in the modeling equations inserted in Table 1 are taken from Nalbant Atak et al. [15].

3.1.2. General conversion equations

Mass and species, energy, and exergy rate balance equations at steady-state conditions are applied to all components used in the integrated plant to determine the thermodynamic properties and exergy destructions of each component.

$$\sum \dot{n}_{in} MW_{in} - \sum \dot{n}_e MW_e = 0 \tag{4}$$

$$\dot{Q}_{cv} - \dot{W}_{cv} + \sum \dot{n}_{in} \bullet \left(\bar{h}_{in} + \frac{V_{in}^2}{2} + g z_{in}\right) - \sum \dot{n}_e \bullet \left(\bar{h}_e + \frac{V_e^2}{2} + g z_e\right) = 0 \tag{5}$$

$$\sum_j \dot{E}_{Q,j} - \dot{W}_{cv} + \sum_i \dot{E}x_{in} - \sum_e \dot{E}x_e - \dot{E}x_D = 0 \tag{6}$$

where the i and e subscripts are denoting the inlet and exit, respectively. $\dot{n}$ and MW are the molar flow rate and the molecular weight, respectively. $\dot{Q}$, $\dot{W}$, and $\bar{h}$ are defined as the heat transfer rate, the work transfer rate, and molar specific enthalpy, respectively. $\dot{E}_{Q,j}$ is the exergy transfer rate due to the heat transfer. $\dot{W}_{cv}$ is the exergy transfer rate due to the work. $\dot{E}x_i$ and $\dot{E}x_e$ are the exergy flow rates with the inlet and exit flows. $\dot{E}x_D$ is the rate of exergy destruction in the control volume.

Table 1
Mass and energy balance equations for the MR reaction and permeation sides.

Sides of MR	Principle	Equations
Reaction Side	Mass and Species Balance	$\frac{d\dot{n}_j^{ret}}{dz} = \rho_b A_c \sum_{i=1}^{3} \vartheta_{i,j} R_j (j = CH_4, CO, CO_2, H_2O)$ $\frac{d\dot{n}_j^{ret}}{dz} = \rho_b A_c \sum_{i=1}^{3} \vartheta_{i,j} R_j - J_{H_2}(2\pi r_{i,o})(j = H_2)$
	Energy Balance	$\sum_{i=1}^{5} \dot{n}_i C_{p,i} \frac{dT_{ret}}{dz} = \rho A_c \sum_{j=1}^{3} \vartheta_{i,j} R_j (-\Delta H_j) + 2\pi \left[r_{o,o} U_{shell} (T_{wall} - T_{ret}) - r_{i,o} U_{tube} (T_{ret} - T_{perm}) \right]$
	Reaction Kinetics	$R_1 = k_{0,1} exp\left(\frac{-E_1}{\overline{R}T}\right) \left[p_{CH_4} p_{H_2O} - \frac{p_{H_2}^3 p_{CO}}{K_{eq,1}} \right] / \left(p_{H_2}^{2.5} \bullet DEN^2 \right) R_2 = k_{0,2} exp\left(\frac{-E_2}{\overline{R}T}\right) \left[p_{CO} p_{H_2O} - \frac{p_{H_2} p_{CO_2}}{K_{eq,2}} \right] / \left(p_{H_2} \bullet DEN^2 \right) R_3 =$ $k_{0,3} exp\left(\frac{-E_3}{\overline{R}T}\right) \left[p_{CH_4} p_{H_2O}^2 - \frac{p_{H_2}^4 p_{CO_2}}{K_{eq,3}} \right] / \left(p_{H_2}^{3.5} \bullet DEN^2 \right) DEN = 1 + K_{CH_4} p_{CH_4} + K_{CO} p_{CO} + K_{H_2} p_{H_2} + K_{H_2O} \frac{p_{H_2O}}{p_{H_2}} K_j = K_{j,0} \bullet exp\left(\frac{-\Delta \overline{h}_i}{\overline{R}T}\right)$
Permeation Side	Mass Balance	$\frac{d\dot{n}_{H_2}^{perm}}{dz} = J_{H_2}(2\pi r_{i,o})$
	Energy Balance	$\sum_{i=1}^{2} \dot{n}_i C_{p,i} \frac{dT_{perm}}{dz} = 2\pi r_{i,o} U_{tube} (T_{ret} - T_{perm})$
	Hydrogen Permeation	Sieverts-Fick Law: $J_{H_2} = \frac{B_{H_2}}{\delta} \left(p_{H_2,ret}^{0.5} - p_{H_2,perm}^{0.5} \right) B_{H_2} = B_{H_2}^0 \bullet exp\left(\frac{-E_m}{\overline{R}T}\right)$

3.2. Thermoeconomic analysis

Thermo-economic analysis combines thermodynamic and economic principles to examine the costs, inefficiencies, and benefits related to the conversion and utilization of energy in a given system [21]. The first step of a thermo-economic analysis is to conduct the economic analysis and, in this regard, the initial cost rate ($\dot{Z}_k$) and the capital recovery factor (CRF) can be calculated as reported below [22]:

$$\dot{Z}_k = \frac{Z_k \cdot CRF \cdot \varphi}{N}, \; Z_k = Z_{ref} \cdot \left(\frac{CEPCI_{2023}}{CEPCI_{base}} \right), CRF = \frac{(i_r \cdot (1 + i_r)^n)}{(1 + i_r)^n + 1}, \tag{7}$$

where φ and N are the maintenance rate (considered as 1.06) and the operation hours per year (considered as 7640 h). Z_k is defined as the purchase equipment cost for each k component, which is calculated by a component cost function given in the Appendix at its reference year and normalized by the cost index (CEPCI). i_r and n are the interest rate (taken as 0.1) and the predicted life of the component (taken as 20 years).

Table 2
Purchase equipment cost of each component in the system.

AUXILIARY COMPONENTS		
Component	**Equation**	**Ref.**
Water pump	$Z_{pump} = 3500 \bullet \dot{W}_{pump}^{0.41}$	[23]
Compressor-1	$Z_{comp\_1} = 91562 \bullet \left(\frac{\dot{W}_{comp-1}}{455} \right)^{2/3}$	[23]
Valve-1	$Z_{valve\_1} = 37 \bullet \left(\frac{P_7}{P_4} \right)^{0.68}$	[24]
Valve-2	$Z_{valve\_2} = 37 \bullet \left(\frac{P_{13}}{P_{11}} \right)^{0.68}$	[24]
Burner	$Z_{burner} = \frac{(46.08 \bullet F_{13} \bullet MW_{air}/1000)}{(0.955 - P_{14}/P_{13})} \bullet (1 + exp(0.018 \bullet T_{14} - 26.14))$	[22]
Boiler	$Z_{boiler} = h_{steam}^{0.8} \bullet \exp\left(\frac{P_{boiler} - 2}{14.29} \right) \bullet exp\left(\frac{T_{boiler} - 350}{446} \right)$	[25]
HEX-1	$Z_{HEX\_1} = 1000 \bullet A_{HEX-1}^{\beta}$	[24]
HEX-2	$Z_{HEX\_2} = 1000 \bullet A_{HEX-2}^{\beta}$	[24]
Blower	$Z_{blower} = 91562 \bullet \left(\frac{\dot{W}_{blower}}{455} \right)^{2/3}$	[26]
MEMBRANE REACTOR SYSTEM		
Component	**Equation**	**Ref.**
Hydrogen Perm-selective Membrane	$Z_{mem\_H_2} = F_p \bullet A_{mem} \bullet C_{mem\_H_2} F_p = B_1 + B_2 \bullet F_m \bullet F_n F_n = a_1 + a_2 \bullet \ln(P_{reac}) + a_3 \bullet \ln(P_{reac})^2 + a_4 \bullet \ln(P_{reac})^6 + a_5 \bullet \ln(P_{reac})^8$	[27]
Catalyst	$Z_{cat} = Vol_{cat} \bullet CR_{cat} Vol_{cat} = (\alpha_{cat} \bullet F_9)/\rho_{cat,kg}$	
Vessel	$Z_{ves} = F_p \bullet C_{ref,reac} \bullet \left(\frac{Vol_{bed}}{Vol_{ref,bed}} \right)^{e_f} Vol_{bed} = Vol_{cat}/(1 - void)$	
Total cost	$Z_{MR} = Z_{mem\_H_2} + Z_{cat} + Z_{ves}$	
CO_2 CAPTURE SYSTEM		
Component	**Equation**	**Ref.**
CO_2 Membrane	$Z_{mem\_CO_2} = A_{mem\_CO_2} \bullet C_{mem\_CO_2}$	[19]
Membrane Frame	$Z_{mem\_fr} = 238 \bullet 10^3 \bullet \left(\frac{A_{mem\_CO_2}}{2000} \right)^{0.7} \bullet \left(\frac{P_{mem}}{55} \right)^{0.88}$	
Compressor-2	$Z_{comp\_2} = F_{17} \bullet 0.0224 \bullet 1.8 \bullet 96 \bullet 10^3$	
HEX-3	$Z_{HEX\_3} = F_{17} \bullet \frac{3.5}{440} \bullet 10^6$	
Total cost	$Z_{Tot\_mem\_CO_2} = Z_{TC\_CO_2} + Z_{O\&M} + Z_{EN} Z_{TC\_CO_2} = (Z_{mem\_fr} + Z_{comp-2} + Z_{HEX-3}) \bullet DF + Z_{mem\_CO_2} \bullet DF_{mem\_CO_2} Z_{O\&M} = 0.01 \bullet \left(Z_{mem_{CO2}} + Z_{mem_{fr}} \right) +$ $0.036 \bullet (Z_{comp-2} + Z_{HEX-3}) Z_{EN} = t_{op} \bullet \left(EC \bullet \dot{W}_{comp_2} \right)$	

Table 2 shows the purchase equipment cost function of each component in the integrated system. Constants used in all purchase equipment cost equations [19,23–27] are given in Table 3.

In the second step, the general cost rate balance equation at the steady state conditions (Eq. (8)) is applied with the calculated capital cost for each component in order to calculate the cost rates of inlet and outlet streams.

$$\left(c_q \dot{E}x_q\right)_k - \left(c_W \dot{W}\right)_k + \sum \left(c \bullet \dot{E}x\right)_{in} - \sum \left(c \bullet \dot{E}x\right)_e + \dot{Z}_k = 0 \quad (8)$$

where $\dot{E}x$ is the rate of exergy defined in the thermodynamic analysis part of this study (Section 3.1.2), c is the cost per unit exergy of the inlet stream (c_i), outlet stream (c_e), heat transfer (c_q), and work (c_W).

Total cost rate of the integrated system ($\dot{C}_{tot}$) can be calculated by using Eq. (9). The latter equation accounts for environmental cost internalization of the system [28], while the environmental cost ($\dot{C}_{env}$) allocation is due to CO and CO_2 and estimated as reported in Eq. (10). It is relevant to note that solid and liquid waste costs are neglected.

$$\dot{C}_{tot} = \sum\nolimits_k \dot{Z}_k + \dot{C}_f + \dot{C}_{D,k} + \dot{C}_{env} \quad (9)$$

$$\dot{C}_{env} = C_{CO}\dot{m}_{CO} + C_{CO_2}\dot{m}_{CO_2} \quad (10)$$

where $\dot{C}_f$ is the fuel cost rate and it can be found using its low heating value ($\dot{C}_f = c_f \dot{m}_f LHV$), $\dot{C}_{D,k}$ is the cost associated with exergy destruction rate ($\dot{C}_{D,k} = \frac{c_{f,k}}{LHV}\dot{E}x_{D,k}$). Here, c_f, $\dot{m}_f$, and LHV are defined as the cost of fuel per unit of energy, mass flow rate of fuel, and low heating value, respectively. $c_{f,k}$ and $\dot{E}x_{D,k}$ are the cost per exergy unit and the exergy destruction rate, respectively. The cost rate balance equations for all components in the integrated system at the steady state condition are reported in Table 4.

4. Results and discussion

4.1. Breakdown analysis

In this section, the major monetary (cost) values associated with the investment, operation, and maintenance to produce hydrogen in the MR are discussed in detail. Fuel, environmental (due to CO and CO_2 releasing), and component costs in addition to those due to non-useful energy (exergy) are analyzed and investigated. The cost breakdown analysis for this system helps to show the economic barriers. The share of the main economic factors is displayed in Fig. 2a and 2b, which describe the analyses carried out with and without CO_2 capture system, respectively.

In the case a CO_2 capture system was considered, the major factor in determining the system cost is found to be fuel cost with a value of 60 %, Fig. 2a. With no effect of environmental costs due to the penalty of flue-gas release to the environment, exergy destruction and component costs account for 34 % and 6 % of the total cost, respectively. On the other hand, when the CO_2 capture system is not included, component and exergy destruction costs decrease while environmental cost increases significantly, Fig. 2b. Moreover, Fig. 2c and 2d show total system and hydrogen production costs. In particular, Fig. 2c shows this trade-off and its effects on the hydrogen cost. Accordingly, the total cost decreases from 260.36 $/h to 239.01$/h (by 8.9 %) when the CO_2 capture system is integrated in the plant, and thus the hydrogen production cost decreases by 12 %. This can be mostly attributed to the environmental costs due to the cost of CO_2 and CO. For example, the system cost is equal to 37.2 $/h in case CO_2 and CO are released from the system, whereas the cost of the carbon-capturing is 9.24 $/h. Overall, the study shows that, from an economic point of view, CO_2 capture integrated system may decrease the cost of hydrogen production for this system. The hydrogen production cost can be reduced further as the carbon social cost likely increases in the following year, according to United States Environmental Protection Agency [29]. Based on that, it is worth of mentioning that the CO_2 capture system is included for the remaining analysis discussed in the next sections.

Table 3
Constants used in all purchase equipment cost equations [19,23–27].

Constant	Value	Constant	Value
$c_{electricity}$	0.0909 $/kWh	c_{water}	0
c_{steam}	11 $/ton	$c_{methane,en}$	3.365 $/GJ
$c_{carbondioxide}$	0.024 $/kg	i_r	0.1
$LHV_{methane}$	55 MJ/kg	φ	1.06
n	20 years	B_2	1.47
B_1	1.62	a_1	0.5146
F_m	1	a_3	0.297
a_2	0.6838	a_5	0.002
a_4	0.0235	$\rho_{cat.kg}$	3460 kg/m^3
α_{cat}	3.59 kg • s/mol	$C_{ref.reac}$	21,936 $
CR_{cat}	10^5 $/m^3	*void*	0.6
$Vol_{ref.bed}$	0.0167 m^3	$C_{mem\_CO_2}$	50 $/m^2
$C_{mem\_H_2}$	3570 $/m^2	DF	0.064
$A_{mem\_CO_2}$	1.094 • 10^3 m^2	t_{op}	8000 h/year
$DF_{mem\_CO_2}$	0.225	β	0.65
EC	0.04 $/kWh	C_{CO_2}	0.024 $/kg
$CEPCI_{2023}$	803.3	C_{CO}	0.0208 $/kg
$CEPCI_{base}$	394		

4.2. The effect of steam-to-carbon (S/C) ratio

The effect of steam-to-carbon (S/C) ratio on the integrated plant is examined thermo-economically. As illustrated in Fig. 3a, the total component cost (purchased cost) increases with increasing S/C. When S/C ratio passes from 1.5 to 4, the total component cost rises by 21 %, whereas the exergy destruction cost decreases by 9.2 %. The major factor of the increasing trend in the total component cost can be explained by the increase in the purchased costs of the MR, boiler, and CO_2 capture system, and the influence of S/C on the major purchased equipment cost is also reported in Table 6. When S/C ratio passes from 1.5 to 4, the increase in the purchased cost of the MR, boiler, and CO_2 capture system is found to be 64 %, 58 %, and 5 %, respectively. The main reason behind this evidence is related to the higher steam flow rate, with a consequent higher components volume. It should be noted that fuel cost does not change with a change in the S/C.

This is due to the assumption of keeping the methane flow rate constant. Therefore, the S/C ratio changes only the steam flow rate, while the methane flow rate is kept constant. In Fig. 3b, the effect of S/C on the hydrogen production cost is shown, evidencing a decreasing trend till achieving ~ 2$/kg$_{H2}$ when the S/C increases from 1.5 to 4. Increasing steam to carbon ratio, component cost increases by 21 %. However, hydrogen production cost decreases by 17 %. This can be due to higher hydrogen production rate with higher steam to carbon ratio. The inset in Fig. 3b shows the aforementioned increasing trend. For example, this accounts for 14 % when S/C passes from 1.5 to 4. It is worth of noting that, when the systems are operated at lower S/C, it is likely to accelerate the carbon formation. However, this phenomenon has been not taken into account in this work.

4.3. The effect of biogas inlet temperature

The effects of biogas inlet temperature on the exergy destruction, component, and hydrogen production costs are displayed in Fig. 4a and 4b, respectively. A slight decrease in component cost is found when the biogas inlet temperature increases. According to the breakdown analysis, the boiler's component cost decreases significantly, while the component cost of the compressor increases slightly. As a result, a change in component cost does not play a major role in determining the hydrogen production cost. Nevertheless, the exergy destruction cost increases with increasing temperature, which results in a change in the

Table 4
Control volume and cost rate balance equations of all components in the integrated system.

Components and Control Volume	Cost Rate Balance Equations	Components and Control Volume	Cost Rate Balance Equations
Water Pump	$\dot{C}_1 - \dot{C}_2 - \left(c_{electricity}\dot{W}_{pump}\right) + \dot{Z}_{pump} = 0$	Valve-1	$\dot{C}_4 - \dot{C}_5 - \dot{C}_6 - \dot{C}_7 + \dot{Z}_{valve\_1} = 0$
Compressor-1	$\dot{C}_6 - \dot{C}_8 - \left(c_{electricity}\dot{W}_{comp\_1}\right) + \dot{Z}_{comp\_1} = 0$	Valve-2	$\dot{C}_{11} - \dot{C}_{12} - \dot{C}_{13} + \dot{Z}_{valve\_2} = 0$
HEX-1	$\dot{C}_{11x} + \dot{C}_{15} - \dot{C}_{11y} - \dot{C}_{15x} + \dot{Z}_{HEX\_1} = 0$	Burner	$\dot{C}_7 + \dot{C}_{13} - \dot{C}_{14} + \dot{Z}_{burner} = 0$
HEX-2	$\dot{C}_{11} + \dot{C}_{22} - \dot{C}_{11x} - \dot{C}_{22x} + \dot{Z}_{HEX\_2} = 0$	Mixer-1	$\dot{C}_3 + \dot{C}_8 - \dot{C}_9 + \dot{Z}_{mixer\_1} = 0$
Membrane Reactor	$\dot{C}_9 + \dot{C}_{14} - \dot{C}_{10} - \dot{C}_{15} - \dot{C}_{22} + \dot{Z}_{MR} = 0$	Mixer-2	$\dot{C}_{15x} + \dot{C}_{10} + \dot{C}_{16} - \dot{C}_{17} + \dot{Z}_{mixer\_2} = 0$
Compressor-2	$\dot{C}_{17} - \dot{C}_{17x} - \left(c_{electricity}\dot{W}_{comp\_2}\right) + \dot{Z}_{comp\_2} = 0$	CO_2 Capture Membrane	$\dot{C}_{17y} - \dot{C}_{18} - \dot{C}_{19} + \dot{Z}_{Tot\_mem\_CO_2} = 0$
HEX-3	$\dot{C}_{17x} - \dot{C}_{17y} + \dot{Z}_{HeX\_3} = 0$	Boiler	$\dot{C}_5 + \dot{C}_{12} + \dot{C}_2 - \dot{C}_{16} - \dot{C}_3 + \dot{Z}_{boiler} = 0$

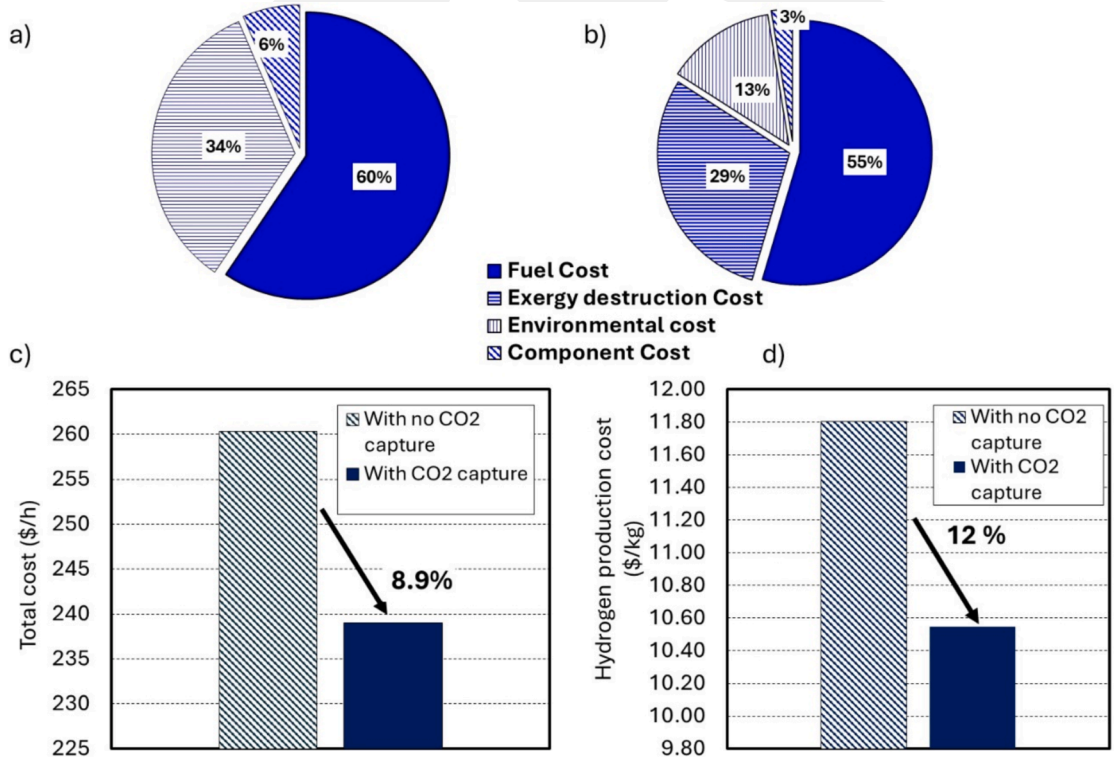

Fig. 2. The share of the main economic factors for the MR-based hydrogen generation system a) without considering CO_2 capturing system, b) with considering CO_2 capturing system, c) overall system costs with and without CO_2 capture, and d) hydrogen production cost with and without CO_2 capturing.

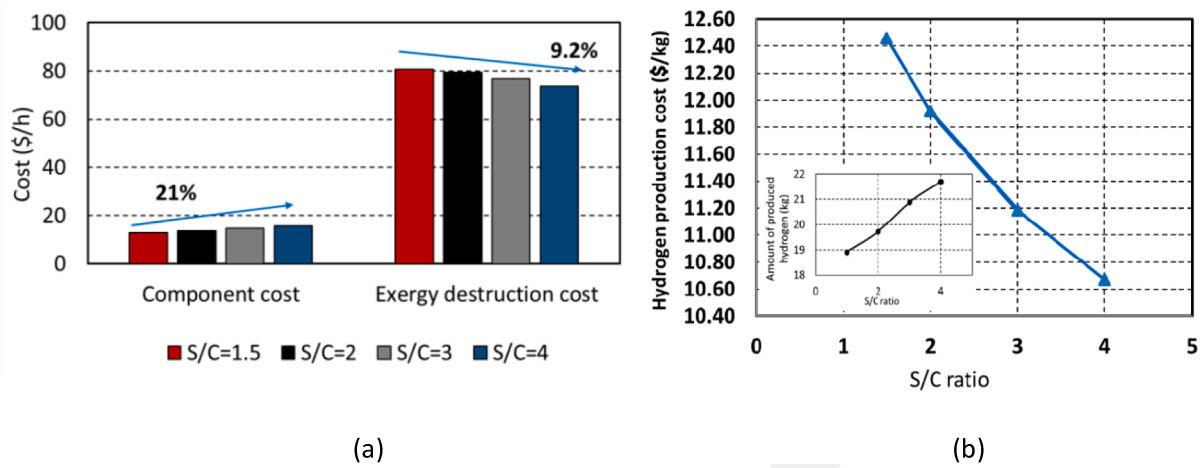

Fig. 3. S/C effect of on a) cost factors and b) hydrogen production cost (Inset: The change of the amount of produced hydrogen with S/C).

Table 6
Influence of S/C on the major purchased equipment cost.

S/C	Equipment cost ($/h)		
	Boiler	Membrane reactor	CO_2 capture system
1.5	1.37	2.43	8.41
2	1.54	2.74	8.50
3	1.87	3.37	8.67
4	2.17	3.99	8.84

hydrogen production cost. As shown in Fig. 4a, passing from 80 $/h for the exergy destruction cost to 100 $/h leads to an increase in the hydrogen production cost by around 7.5 %.

However, there is an extraordinary jump in cost for a temperature range of 400—450 °C of biogas inlet temperature. For example, exergy destruction cost increases only by 1.5 % when the temperature increases from 350 to 400 °C, whereas this increase is found as 25 % when the temperature increases from 400 to 450 °C. The reason for sharp changes in enthalpy, entropy, and exergy occurring specifically at 400–450 °C, rather than in the 300–400 °C, can be explained by the fact that, at higher temperatures, gases achieve a point where molecular motion significantly increases, and certain chemical reactions, phase transitions, or dissociation processes may begin to occur. This results in a more pronounced change in energy and disorder at the higher temperature range, which doesn't happen as sharply between 300–400 °C. Essentially, 400–450 °C might be the threshold where these processes become more noticeable. It can be explained by considering that the exergy destruction rate is limited thermodynamically by the changes in enthalpy ($\Delta H_{T_2} = (\Delta H_{T_1} + \Delta c_p(T_2 - T_1)$ [30]). According to our analysis, the enthalpy of methane increment sharply increases when the temperature increases, while the increase in enthalpy of CO is limited with temperature. According to Fig. 4b, the hydrogen production cost increases from 10.6 $/kg$_{H2}$ to 11.3 $/kg$_{H2}$ in the same temperature range. To better explain this result, exergy analysis applied around the control volume of the boiler is displayed in the inset of Fig. 4b. In this regard, the change in exergy destruction cost mimics the trend of exergy destruction rate for the same temperature range. It is worth recalling one of the main assumptions done in this work, in which the reactor inlet temperature is kept constant. Therefore, the cost of the MR is not influenced by biogas inlet temperature, whereas the boiler is one of the major affected components. These results demonstrate that exergy does not only play a role in defining available energy but also has a significant impact on the cost value of the energy carrier because the customer purchases a useful part of energy.

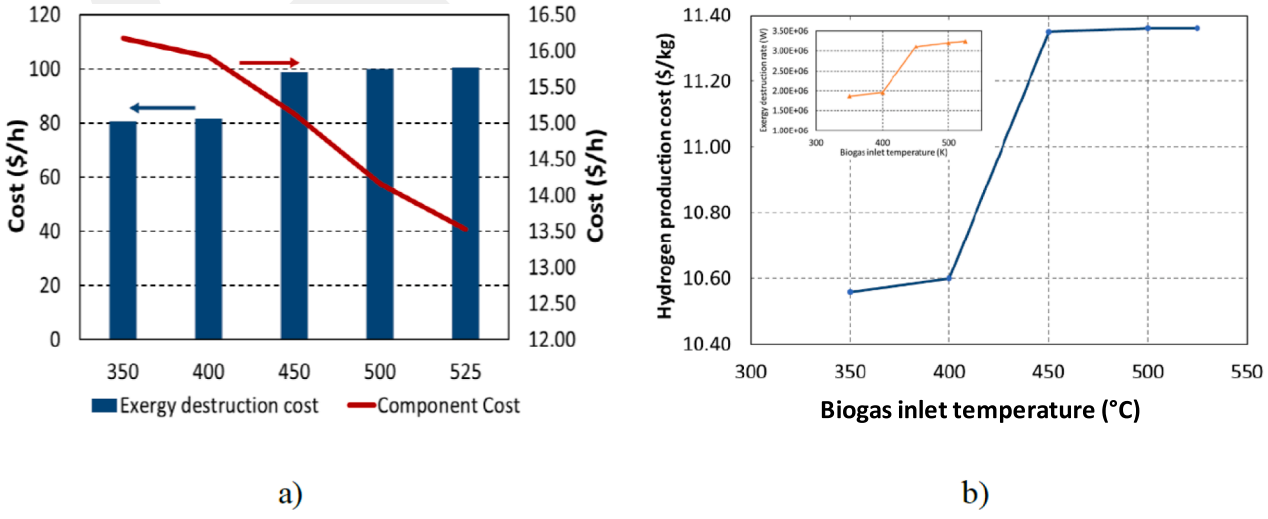

Fig. 4. The effect of biogas inlet temperature on a) cost factors and b) hydrogen production cost (Inset: A change of exergy destruction rate with changing biogas inlet temperature).

5. Conclusions

In this study, a detailed thermo-economic analysis of an integrated plant including a MR-based hydrogen production and a CO_2 capture system is conducted. This plant has the capability of producing highly pure hydrogen from biogas using a MR housing a hydrogen perm-selective membrane, meanwhile concentrating in CO_2 the unpermeated stream to be successively captured in a second stage process. Firstly, the system's economic performance with or without the CO_2 capture system is examined with breakdown analyses. Then, the effects of two important operating parameters such as S/C ratio and biogas inlet temperature on the hydrogen production cost have been investigated. According to the results, it has been confirmed that fuel cost is the major economic factor for hydrogen production cost. The study also showed that environmental and exergy destruction costs can be important economic components, highlighting how the economic cost to implement a CO_2 capture system is more advantageous compared to the plant option without CO_2 capturing feature. Furthermore, this work evidenced that exhausted CO and CO_2 rate lead to environmental cost equal to 37.2 $/h, whereas the cost rate of capturing system is found as 9.24 $/h. Based on that, the utilization of a membrane-based CO_2 capture system can decrease hydrogen production costs by 12 % because of the reduced cost of penalty related to the releasing of greenhouse gases (CO and CO_2). It has been also demonstrated that S/C can deplete hydrogen production costs. When S/C rises from 1.5 to 4, the cost for producing 1 kg of hydrogen can be reduced by approximately 2$ due to lower exergy destruction costs and a higher amount of hydrogen produced. Biogas inlet temperature has been demonstrated to influence the cost of hydrogen produced. When it increases by 50 °C, the cost of 1 kg of hydrogen production increases from $10.6 to $11.3.

In the future, the effect of an optimized thermal integration system (*via* the heat exchanger network) on the total cost of hydrogen production will be examined in detail to reveal some potential cost reduction mechanisms.

CRediT authorship contribution statement

Yagmur Nalbant Atak: Writing – original draft, Investigation, Data curation. **Alper Can Ince:** Writing – original draft, Methodology, Formal analysis, Data curation. **C.Ozgur Colpan:** Writing – original draft, Supervision, Project administration, Conceptualization. **Adolfo Iulianelli:** Writing – original draft, Investigation, Conceptualization, Funding acquisition. **Mustafa Fazil Serincan:** Validation, Methodology, Data curation. **Ugur Pasaogullari:** Visualization, Supervision, Project administration.

Declaration of competing interest

The authors declare that they have no known competing financial interests or personal relationships that could have appeared to influence the work reported in this paper.

Acknowledgement

European Union – NextGeneration EU from the Italian Ministry of Ambient and Energy Security POR H2 AdP MASE/ENEA with involvement of CNR and RSE, PNRR - Mission 2, Component 2, Investment 3.5 "Ricerca e sviluppo sull'idrogeno" project is acknowledged to support this work.

Data availability

Data will be made available on request.

References

[1] IEA (2019). The Future of Hydrogen: Seizing today's opportunities, report prepared by the IEA for the G20, Japan.
[2] Dawood F, Anda M, Shafiullah GM. Hydrogen production for energy: An overview. Int J Hydrogen Energy 2020;45(7):3847–69.
[3] Ince AC, Colpan CO, Keles A, Serincan MF, Pasaogullari U. Scaling and performance assessment of power-to-methane system based on an operation scenario. Fuel 2023;332:126182.
[4] Mamivand, S., Binazadeh, M., Sohrabi, R. (2021). Applicability of membrane reactor technology in industrial hydrogen producing reactions: Current effort and future directions.Journal of Industrial and Engineering Chemistry, 104, 212-230.
[5] Nalbant Atak Y, Colpan CO, Iulianelli A. A review on mathematical modeling of packed bed membrane reactors for hydrogen production from methane. Int J Energy Res 2021;45(15):20601–33.
[6] Binazadeh M, Mamivand S, Sohrabi R, Taghvaei H, Iulianelli A. Membrane Reactors for Hydrogen Generation: from Single Stage to Integrated Systems. Int J Hydrogen Energy 2023;48:39225–53.
[7] Amiri TY, Ghasemzageh K, Iulianelli A. Membrane reactors for sustainable hydrogen production through steam reforming of hydrocarbons: A review. Chemical Engineering and Processing-Process Intensification 2020;157:108148.
[8] Ma LC, Castro-Dominguez B, Kazantzis NK, Ma YH. Integration of membrane technology into hydrogen production plants with CO_2 capture: An economic performance assessment study. Int J Greenhouse Gas Control 2015;42:424–38.
[9] Liguori S, Kian K, Buggy N, Anzelmo BH, Wilcox J. Opportunities and challenges of low-carbon hydrogen via metallic membranes. Progress Energy Combustion Science 2020;80:100851.
[10] Elavarasan RM, Pugazhendhi R, Irfan M, Mihet-Popa L, Khan IA, Campana PE. State-of-the-art sustainable approaches for deeper decarbonization in Europe–An endowment to climate neutral vision. Renew Sustain Energy Rev 2022;159:112204.
[11] Wu HC, Rui Z, Lin JY. Hydrogen production with carbon dioxide capture by dual-phase ceramic-carbonate membrane reactor via steam reforming of methane. J Membr Sci 2020;598:117780.
[12] Basile A, Gallucci F, Iulianelli A, Tosti S. CO-free hydrogen production by ethanol steam reforming in a Pd-Ag membrane reactor. Fuel Cells 2008;8:62–8.
[13] Kim CH, Han JY, Lim H, Lee KY, Ryi SK. Methane steam reforming using a membrane reactor equipped with a Pd-based composite membrane for effective hydrogen production. Int J Hydrogen Energy 2018;43(11):5863–72.
[14] Shirasaki Y, Yasuda I. Membrane reactor for hydrogen production from natural gas at the Tokyo Gas Company: A case study. In: Handbook of Membrane Reactors. Woodhead Publishing; 2013. p. 487–507.
[15] Atak YN, Colpan CO, Iulianelli A. Energy and exergy analyses of an integrated membrane reactor and CO_2 capture system to generate decarbonized hydrogen. Energ Conver Manage 2022;272:116367.
[16] Lee H, Lee B, Byun M, Lim H. Comparative techno-economic analysis for steam methane reforming in a sorption-enhanced membrane reactor: Simultaneous H_2 production and CO_2 capture. Chem Eng Res Des 2021;171:383–94.
[17] Mikulčić H, Skov IR, Dominković DF, Alwi SRW, Manan ZA, Tan R, et al. Flexible Carbon Capture and Utilization technologies in future energy systems and the utilization pathways of captured CO_2. Renew Sustain Energy Rev 2019;114:109338.
[18] Ghasemzadeh K, Morrone P, Iulianelli A, Liguori S, Babaluo AA, Basile A. H_2 production in silica membrane reactor via methanol steam reforming: modeling and HAZOP analysis. Int J Hydrogen Energ 2013;38:10315–26.
[19] Asadi J, Kazempoor P. Techno-economic analysis of membrane-based processes for flexible CO_2 capturing from power plants. Energ Conver Manage 2021;246:114633.
[20] Jabbari B, Jalilnejad E, Ghasemzadeh K, Iulianelli A. Recent progresses in application of membrane bioreactors in production of bio-hydrogen. Membranes 2019;9:100.
[21] Valero A, Torres C. Thermoeconomic analysis. Exergy, energy system analysis and optimization 2006;2:1–35.
[22] Dincer I, Rosen MA, Ahmadi P. Optimization of energy systems. John Wiley & Sons; 2017.
[23] Peters MS, Timmerhaus KD, West RE, Timmerhaus K, West R. Plant Design and Economics for Chemical Engineers. New York: McGraw-Hill; 1968.
[24] Ahmadi P, Dincer I. Thermodynamic analysis and thermoeconomic optimization of a dual pressure combined cycle power plant with a supplementary firing unit. Energ Conver Manage 2011;52(5):2296–308.
[25] Silveira JL, Tuna CE. Thermoeconomic analysis method for optimization of combined heat and power systems. Part I. Progress in energy and Combustion. Science 2003;29(6):479–85.
[26] Chen Y, Niroumandi H, Duan Y. Thermodynamic and economic analyses of a syngas-fueled high-temperature fuel cell with recycling processes in novel electricity and freshwater cogeneration plant. Energy 2021;235:121313.
[27] Sanusi YS, Mokheimer EM. Thermo-economic optimization of hydrogen production in a membrane-SMR integrated to ITM-oxy-combustion plant using genetic algorithm. Appl Energy 2019;235:164–76.
[28] de Faria PR, Barone MA, dos Santos RG, Santos JJC. The environment as a thermoeconomic diagram device for the systematic and automatic waste and

environmental cost internalization in thermal systems. Renew Sustain Energy Rev 2023;171:113011.
[29] The Social Cost of Carbon. (2017). United States Environmental Protection Agency. https://19january2017snapshot.epa.gov/climatechange/social-cost-carbon_.html.
[30] Moran MJ, Shapiro HN, Boettner DD, Bailey MB. Fundamentals of engineering thermodynamics. Chichester - England: John Wiley & Sons Ltd; 2010. p. 1–831.